COBEM 2023 27TH INTERNATIONAL CONGRESS OF MECHANICAL ENGENEERING

ABCM Brazilian Society of Mechanical Sciences and Engineering
27th ABCM International Congress of Mechanical Engineering
December 04-08, 2023, Florianópolis-SC, Brazil

COB-2023-0871
THEORETICAL AND EXPERIMENTAL ANALYSIS OF A HYBRID SOLAR-ELECTRIC DRYER

Gabriel M. B. Cruz
Vinicius Augusto Camatta Santana
Frederico Carlos Moraes Hippert Soares
Bárbara Caroline Ricci Nunes
Cristiana Brasil Maia
Pontifícia Universidade Católica de Minas Gerais, Av. Dom José Gaspar, 500, 30535-901 – Belo Horizonte – MG
E-mail: gabrielmbc98@gmail.com, viniciusbh@msn.com, fredericohippert@gmail.com, barbararicci@sga.pucminas.br, cristiana@pucminas.br

Abstract. *Solar energy is a feasible option for developing sustainable technologies since it is a free and abundant energy source. Hybrid solar dryers use solar energy as a primary source combined with a complementary source when needed. It ensures a stable and manageable drying process that produces high-quality dried food. However, hybrid dryers usually require a higher initial investment. This paper aims to present a mathematical model using Engineering Equation Solver (EES) software to predict the behavior of the drying air to aid project development. It was possible to analyze the thermal efficiency and the airflow temperature in a hybrid solar-electric dryer without load. The methodology is theoretical and experimental driven. The theoretical modeling study analyzes the temperatures and efficiency of the dryer, based on the First Law of Thermodynamics and solar engineering of thermal processes. It was possible to compare the results and validate the model by using experimental data of temperature, solar radiation, and wind speed measured at an experimental prototype in Belo Horizonte, Brazil. Five cases study were developed, with satisfactory results, ranging from 0,4% to 13,1% of error. Each of those cases relies less on measured data. The geometry influence on the predicted values was exemplified to assess the algorithm's performance.*

Keywords: *hybrid solar-electric drying, solar engineering, energetic analysis, solar collector modeling.*

1. INTRODUCTION

One of the most used methods for food preservation worldwide is dehydration. The moisture content in the food creates a favorable environment for microorganism proliferation, such as molds, bacteria, and yeasts. Therefore, removing this water content will increase the shelf-life of the food and add value to the product. Since solar energy is a free and abundant energy source, one of the oldest and cheapest methods for dehydration is sun drying, which consists of the exposure of thin layers of food in trays under direct sunlight and wind. However, this method does not protect the product from rain, insects, or animals. Besides that, the drying behavior completely depends on weather conditions, resulting in an unmanageable process (Mühlbauer and Müller, 2020). The intermittent nature of the solar resource, due to rainy or cloudy days, poses a challenge for the continuous operation of conventional solar dryers. Researchers have introduced hybrid solar drying as an alternative approach to address the disrupted nature of solar drying. Hybrid solar dryers can utilize an auxiliary energy resource, such as electric (Hadibi et al., 2021) or biomass (Dhanushkodi et al., 2017) backup heaters, in addition to solar energy, to heat the drying air. This approach aims to improve the drying process by minimizing the effects of intermittent solar energy (Dake et al., 2021).

In recent years, different types of hybrid dryers have been studied to be applied in small- or large-scale production. However, not only vegetables and fruit drying are analyzed. For instance, some recent studies investigated the drying behavior and performance of fish drying, such as Bombay duck and shrimp, using hybrid dryers (Murali et al. 2022; Alfiya et al. 2022). Besides that, hybrid dryers can have different shapes and work principles. For example, Malakar et al. (2022) studied the thermal performance of beetroot drying using a solar dryer, in which an evacuated tube solar collector is used to heat the air. Another example is the work of Roratto et al. (2021), who analyzed a hybrid-solar-vacuum dryer with a drying chamber operating under vacuum or vacuum pulses.

Furthermore, extensive research has been conducted on thermal storage in solar dryers to enhance the efficiency and effectiveness of solar drying. The primary objective of thermal storage in solar dryers is to incorporate a way to accumulate heat during periods of high solar radiation to be used during periods of low solar radiation to maintain a stable and continuous drying process. Using thermal energy storage material makes it possible to continue the drying process for approximately 3 hours after the sunshine hours and obtain products of higher quality due to the uniform drying (Bhavshar and Patel, 2023). Most studies on thermal storage have focused primarily on latent and sensible heat storage (Dake et al., 2021).

The main focus of this study is to develop and analyze a flexible drying model and a mathematical algorithm to analyze the air heater for hybrid dryer projects. Therefore, the outflow air properties from a Hybrid Solar-Electric Dryer (HSED) developed by Barbosa et al. (2018) were studied to validate this modeling method. The numerical results of the outflow air temperature are compared with the measured data, which is considered the accepted value. An algorithm to estimate local insolation and calculate the desired temperatures and thermal efficiency was developed. In this work, five case studies were considered in which the final airflow temperature is computed. The cases differ from one another by using each time more experimental data parameters instead of standardized values or estimations. Therefore, the percentage error is expected to decrease when more measured data are used as the input for the algorithm. However, the reliance on more measured data requires more equipment and study time to perform data acquisition. Besides, geometry optimization is overviewed to exemplify the use of the algorithm for design development.

2. MATERIALS AND METHODS

In this study, an algorithm was developed to estimate local insolation and the temperature of the air exiting the solar collector of the HSED without load. To validate the thermal model, the results were compared with measured data. The main objective of this numerical study is to obtain a way to evaluate the performance of the air heater before building the dryer. This study can be used to optimize future dryer structure designs by testing different geometrical characteristics or materials used. Besides, it is possible to analyze the heater's performance during different seasons of the year at any location.

Five case studies were considered in this work, which all calculate the final airflow temperature. Each of those cases relies progressively less on measured environmental data, meaning that it is expected to have a decrease in precision on the estimations over each case. However, the reliance on more measured data requires more equipment and study time to perform data acquisition.

Case 1 uses measured ambient temperature, inlet air temperature, and insolation data as input. This case study is possible if the dryer is already built. Case 2 uses the same temperature data but with standardized insolation data, which is useful if no insolation meter is available for experiment measurement. Case 3 uses measured ambient temperature, estimated inlet temperature, and standard insolation data. This case can be useful for developing dryer projects or with limited sensors. Case 4 uses measured ambient, estimated inlet temperature, and estimated insolation. If no insolation standard data is available, this study case can be used to estimate the insolation based only on the dryer's geographical location. Finally, Case 5 relies only on standard temperature data. Therefore, the inlet temperature and insolation are estimated in this case.

The standard ambient temperature data were based on the Typical Meteorological Year (TMY) developed by the project entitled Solar and Wind Energy Resource Assessment (SWERA) (Martins et al., 2007). This project aims at assembling high-quality information on solar and wind energy resources by determining the standard year for several Brazilian cities, including Belo Horizonte. The TMY is a dataset of climatological parameters for one year representing the most likely scenario for the desired parameters. Thus, the data present the standard year consisting of 12 months individually selected from a historical series of approximately 23 years (Crawley and Huang, 1997).

The insolation estimation was calculated by the methods developed by Erbs et al. (1982), which is described and compared in detail with other methods by Duffie and Beckman (2013). In this study, it is considered an isotropic sky model. The radiation on the air heater surface includes three components: beam, isotropic diffuse, and solar radiation diffusely reflected from the ground. To estimate the insolation, it is necessary to know the geometric characteristics of the solar collector and the materials properties used to build it. Besides, this method takes into consideration the path of the sun. Therefore, it is necessary also to know the latitude and longitude values of the dryer's location and the desired date and time.

To compare the numerical results, the hourly percentage error was calculated in each case, as demonstrated by Eq. (1).

$$\%Error = \frac{Tf_{calculated} - Tf_{measured}}{Tf_{measured}} \cdot 100\%. \quad (1)$$

The experiments were carried out off-load with natural convection mode and without using the auxiliary energy source. The experimental work was performed between 7 and 9 of June 2023. 3 days analysis was chosen to highlight the influence of the adversities of the climate.

2.1 Experimental Setup and Instrumentation

The Hybrid Solar-Electric Dryer is located at the Renewable Energy Studies Group (GREEN) at the Pontifical Catholic University of Minas Gerais, Belo Horizonte, MG, Brazil (latitude 19.92 °S and longitude 43.99 °W). Barbosa et al. (2018) first developed the dryer studied in this work for a banana drying experimental analysis. The dryer is equipped with several sensors for performance analyses. Since experimental studies are subjected to errors of different natures, uncertainty analyses of the HSED were conducted.

The HSED is divided into a solar collector, which is tilted 30º from the horizontal, and a drying chamber where the products are dried and where the electric heater is located. The solar collector is 1.74 m long, 1.30 m wide, and 0.35 m deep, with a cover glass on top 6 mm thick. The drying chamber is 0.89 m long, 1.30 m wide, and 1.20 m high, with a cover glass 6 mm thick on top and on one side. The walls of the HSED are made with galvanized steel plates painted in matte black to increase their absorptance. There is a chimney 0.35 m high with 0.20 m of diameter on top of the dryer to allow the drying air to exit. The exit of the chimney has a funnel shape that tapers down to a 0.05 m diameter to facilitate air velocity data collection exiting the dryer. A schematic drawing is presented in Figure 1 with the dryer's dimensions. Two doors on the back of the drying chamber allow access inside the dryer to introduce and remove trays 0.75 m long and 0.50 m wide. The left side of the chamber can accommodate up to four fixed trays, while the right side has two options: it can accommodate up to two fixed trays, or only one tray suspended by a wire connected to a load cell.

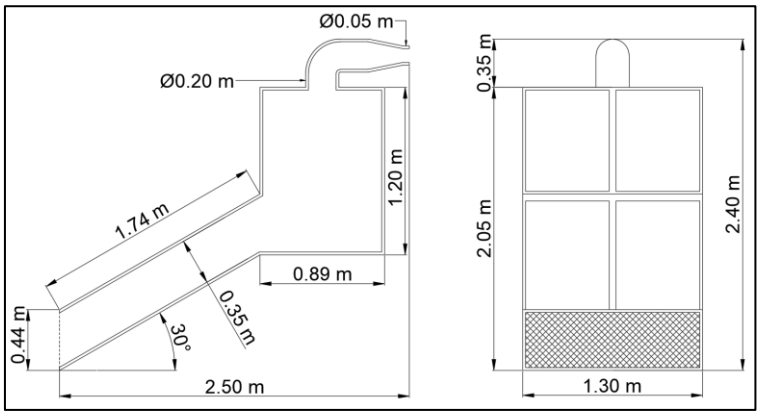

Figure 1. Schematic of the dryer.

The data acquisition system and the heater control can be monitored remotely on the supervisory system software ScadaBR through a Python script. The data can be downloaded on a computer and saved on a Secure Digital card as a backup.

All of the sensors used are described in Table 1 and are set as demonstrated in Figure 2. The accuracy described is the maximum error recorded at the end of the measurement scale.

Table 1. Specifications of sensors used in HSED.

Model no.	DS18B20	DHT11	DHT22 Am2302	DHT21 Am2301
Parameters	Temperature	Temperature and humidity	Temperature and humidity	Temperature and humidity
Range	-55 to 125 °C	0 to 50 °C 20 to 90 % RH	-40 to 80 °C 0 to 100 % RH	-40 to 80 °C 0 to 99.9 % RH
Accuracy	± 0.5 °C	± 2.0 °C ± 5.0 % RH	± 0,5 °C ± 2.0 % RH	± 0,5 °C ± 3.0 % RH
Quantity	6	1	1	1
Caption	S1 to S6	S7	S8	S9

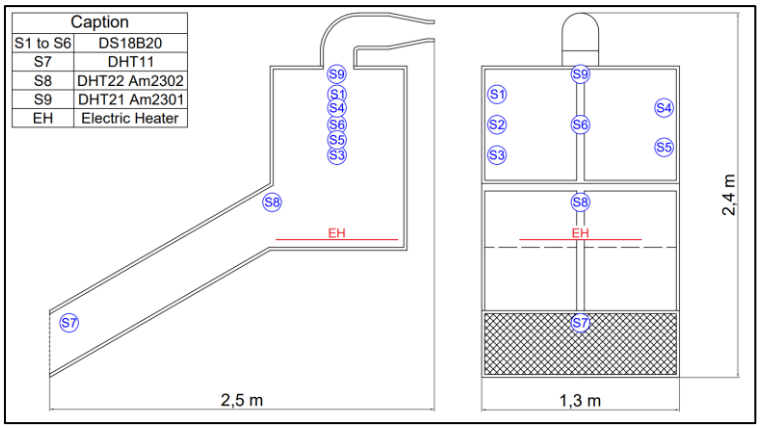

Figure 2. Schematic of sensor and electric heater location in the dryer.

An anemometer was installed at the exit of the chimney to collect air velocity data. The anemometer model is Gm8903, with an operating range between 0 to 30 m/s and an accuracy of 0.09 m/s at the end of the scale. Besides, at the entry of the chimney, a 120 mm diameter cooler is installed to change the air velocity exiting the dryer.

The meteorological data were measured by GREEN's weather station, located less than a 50 m radius from the HSED. Irradiation, precipitation, and ambient temperature data were measured using a standardized PV reference cell, a thermometer, and a rain gauge. The PV reference cell and the thermometer are part of an irradiance measurement system (RDE 300 series) produced by Atonometrics. The reference cell was calibrated at both 1000 W/m^2 and 135 W/m^2. A wash unit is located on top of the sensor, and it automatically sprays water to remove excess soiling and dust. The irradiance uncertainty is ± 2,0% at 1000 W/m2. The thermometer used is a Pt1000 RTD thermometer, with an uncertainty of ± 0,1 °C.

The dryer has an electronic control system to measure temperature and relative humidity at several locations within it. The control panel contains an Arduino Mega, a solid-state relay, and other electronic and protection devices. To have a manageable drying process and a stable temperature inside the drying chamber, there is an electric heater that can be activated manually or automatically. The data acquisition system and the heater control can be monitored remotely on the supervisory system software ScadaBR through a Python script. The data can be downloaded onto a computer and saved on a Secure Digital card as a backup.

2.1.1 Uncertainty analyses

According to Akpinar (2010), the uncertainty and errors in experiments can result from the instrument selection, condition, calibration, environment, observation, reading, and test planning. To evaluate the uncertainty in the results of drying experiments in solar dryers, the author proposed a method used as a base in this section. This method proved to be suitable for uncertainty analysis in drying technologies in past research (Tiwari and Tiwari, 2016; Chauhan et al., 2018). Since all the data was collected directly by the software ScadaBR, the reading uncertainties were neglected.

The temperature measurement total uncertainty, $u_{Temperature}$, can be estimated with Eq. (2) with the accuracy values of the thermometers previously presented in Table 1.

$$\begin{aligned} u_{Temperature} &= [6 \cdot (u_{\mathrm{DS18B20}})^2 + (u_{\mathrm{DHT11}})^2 + (u_{\mathrm{DHT22}})^2 + (u_{\mathrm{DHT21}})^2 + (u_{RTD})^2]^{1/2}, \\ &= [6 \cdot 0.5^2 + 2^2 + 0.5^2 + 0.5^2 + 0.1^2]^{1/2} = 2.45\ °C, \end{aligned} \tag{2}$$

in which the subscripts $DS18B20$, $DHT11$, $DHT22$, $DHT21$, RTD are the sensors models.

The air velocity measurement total uncertainty, $u_{Humidity}$, can be estimated with Eq. (3). Notice that the air leaking uncertainty is a general estimation proposed by Akpinar (2010).

$$\begin{aligned} u_{Air\ velocity} &= [(u_{anemometer})^2 + (u_{leak})^2]^{1/2}, \\ &= [0{,}09^2 + 0{,}1^2]^{1/2} = 0{,}13\ m/s. \end{aligned} \tag{3}$$

Furthermore, the total uncertainty for the final temperature estimation, $Temperature_{est}$, for the solar heater can be calculated as in Eq. (4).

$$\begin{aligned} u_{Temperature_{est}} &= \left[\left(u_{Temperature}\right)^2 + \left(u_{Air\ velocity}\right)^2 + (u_{Irradiance})^2\right]^{1/2}, \\ &= [2{,}45^2 + 0{,}13^2 + 0{,}02^2]^{1/2} = 2{,}45\ \%. \end{aligned} \tag{4}$$

2.2 Dryer modeling

The dryer model proposed was developed based on Duffie and Beckman (2013). To determine the changes produced in the properties of the air, an algorithm was developed with Engineering Equation Solver (EES) software to estimate the heat transfer coefficients and the temperatures related to the dryer. The energy balance and the thermal network proposed are demonstrated in Figure 3a-b. The algorithm methodology is similar to past studies (Cruz and Maia, 2022), but in this paper, the algorithm was optimized and executed using different software, in which the properties of the air can be automatically calculated and changed in between each iteration, obtaining a considerably lower error. Besides, an in-depth analysis of the influence on the input data is assessed in this paper to evaluate the model, and the predictions are executed for a different season in which the climate conditions have higher predictability.

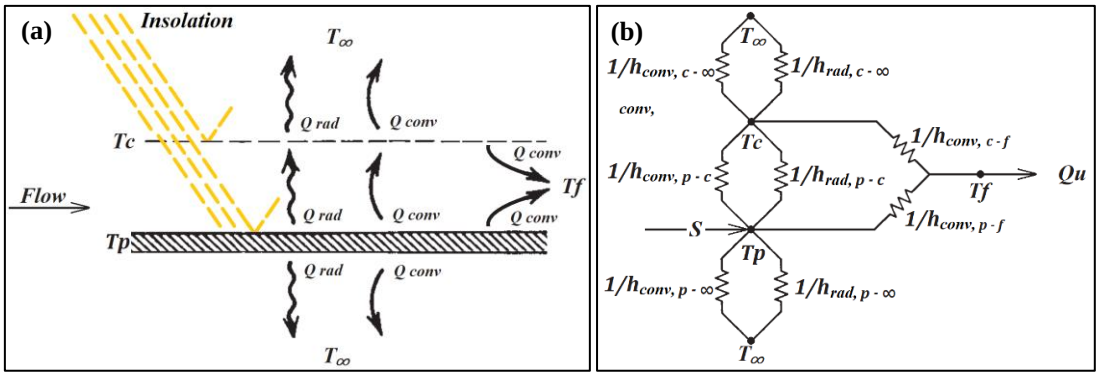

Figure 3. (a) Energy balance in the collector and (b) thermal network.

The absorbed radiation by the plate, S, can be estimated from Eq. (5), in which the total incident radiation, I, is given by the sum of three components: a share of direct beam radiation, I_b, a portion of diffuse radiation, I_d, and a portion of radiation reflected by the soil and environment surrounding the dryer, I_g (Duffie and Beckman 2013). The term β represents the angle between the plane of the surface in question, and the horizontal, which is normally equal to the latitude where the collector is installed, and ρ_g represents the reflectivity of the ground. The geometric factor R_b represents the ratio of beam radiation on the tilted surface to that on a horizontal surface at any time.

$$S = I_b\, R_b(\tau\alpha)_b + I_d(\tau\alpha)_d \left(\frac{1+\cos\beta}{2}\right) + \rho_g\, I(\tau\alpha)_g \left(\frac{1-\cos\beta}{2}\right). \tag{5}$$

The term $(\tau\alpha)$ given by Eq. (6) represents the product of transmittance and absorptance values for the direct beam, diffuse, and ground radiation parcels, with the subscripts b, d, and g respectively.

$$(\tau\alpha) = \frac{\tau\alpha}{1-(1-\alpha)\rho_d}. \tag{6}$$

The performance of a solar collector is usually described by an energy balance, considering the distribution of incident solar energy into useful energy gain, Q_u, thermal losses, and optical losses. It is possible to estimate the useful energy gain with Eq. (7). Note that F' and F'' are the collector efficiency factor and the collector flow factor, respectively. The thermal losses from the collector to the surrounding occur by conduction, convection, and infrared radiation, which all are considered when calculating the total heat transfer coefficient, U_L. The maximum possible useful energy gain in a solar collector happens when the whole collector is at the inlet fluid temperature, T_i.

$$Q_u = A_c\, F'F''[S - U_L(T_i - T_a)]. \tag{7}$$

The main difference between a thermal network and an electrical network is that while the electric resistance does not change when the voltage varies, the thermal resistance does change when the temperature varies. This occurs because the thermal resistance depends on the heat transfer coefficient, which depends on the boundary temperatures. Therefore, the algorithm developed to solve the proposed thermal network has an iterative process to determine the desired temperatures.

Until now, the glass cover temperature, T_c, was an estimated value. However, with Eq. (8), it is possible to recalculate T_c. Then, after calculating the new cover temperature, all the thermal resistance is recalculated.

$$T_c = T_p - \frac{U_t(T_p - T_a)}{U_{pc}}, \tag{8}$$

in which U_t is the overall top heat transfer coefficient, and U_{pc} is the overall plate-cover heat transfer coefficient.

Next, it is possible to determine a new outflow air temperature, T_f, with Eq. (9).

$$T_f = Ti + \frac{Q_u}{\dot{m}\, Cp}. \tag{9}$$

Since the plate temperature, T_p, was an estimated value until now, it can be recalculated knowing the new outflow temperature with Eq. (10)

$$T_p = T_f + \frac{Q_u(1-F'F'')}{A_c\, F'\, F''\, U_L}. \tag{10}$$

After calculating the overall heat transfer coefficient between the collector and the outflow air, it is possible to calculate the final outflow air temperature, Eq. (11), and the dryer's efficiency, Eq. (12).

$$T_f = T_p - \frac{U_f\,(Tp-Tc)}{U_{pc}}. \tag{11}$$

$$\eta = \frac{\dot{m}\, Cp\,(Tf-Ta)}{S}. \tag{12}$$

At last, an iterative process takes place until the temperature value converges.

3. RESULTS AND DISCUSSION

An algorithm was developed to calculate the temperatures related to the air heater from a Hybrid Solar-Electric Dryer. However, some inputs are required, such as the geometric properties of the heater, optical properties of the materials (transmittance, reflectance, and absorptance), a theoretical mass flow rate, and the climate data.

This study was divided into five cases, summarized in Tab. 2.

Table 2. Summary of all cases studied.

	Ambient temperature, Ta	Inlet temperature, Ti	Insolation, I	Airflow velocity
Case 1	Measured	Measured	Measured	Measured
Case 2	Measured	Measured	Standard	Estimated
Case 3	Measured	Estimated	Standard	Estimated
Case 4	Measured	Estimated	Estimated	Estimated
Case 5	Standard	Estimated	Estimated	Estimated

Firstly, the measured temperatures (ambient, inlet, and outlet airflow) and the standard ambient temperature based on the TMY are presented in Fig. 4a, the insolation input is presented in Fig. 4b, and the measured outlet airflow velocity is in Fig. 5.

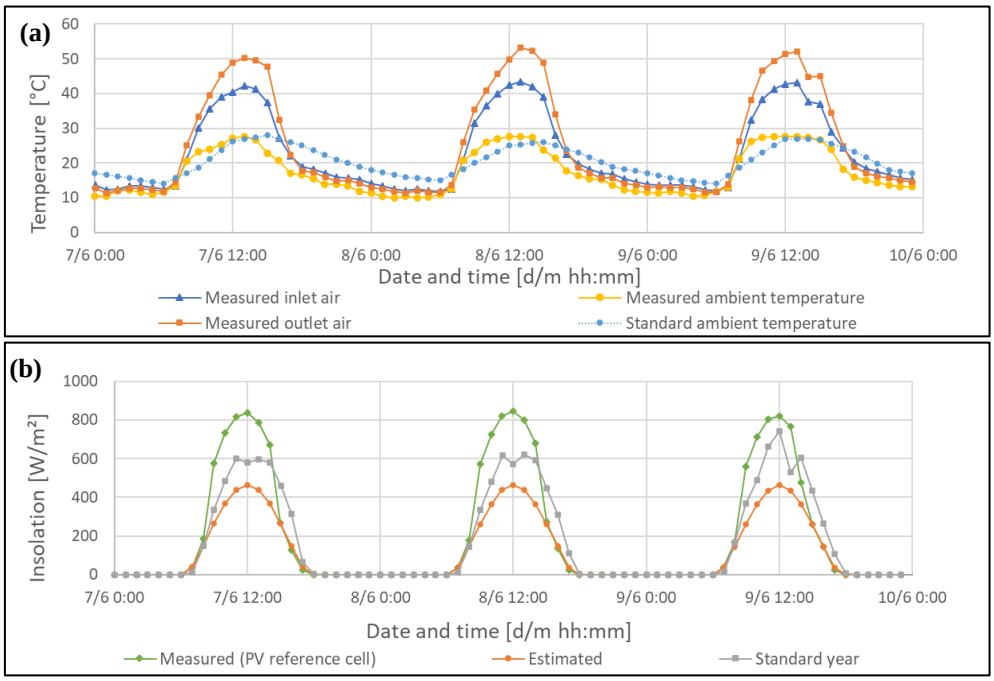

Figure 4. (a) Temperatures and (b) insolation data.

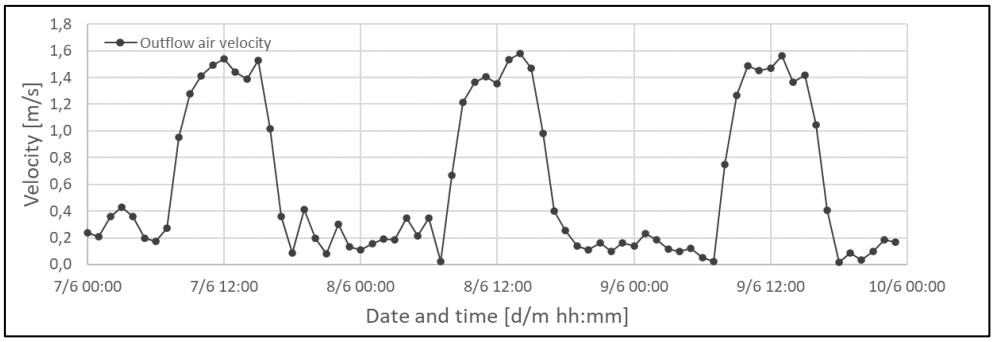

Figure 5. Outflow air velocity measured data.

Note in Fig. 4a that the dryer increased the temperature up to 10.4 ℃ around 13:00 - 15:00. When analyzing the ambient temperature, the standard temperature was similar to the measured data, but during the night the measured temperature is lower. This probably happened due to measurement location, since the dryer is located near a hill, the wind could have lowered the temperature. However, since this study is applied for solar dryer analysis, the results during the night were not considered for error analysis.

In Fig. 4b, there is a high discrepancy between the measured insolation with the estimated, with the standard insolation values in between both. The PV reference cell is located in a solar collector a few meters from the dryer. However, after 15:00, it is possible to see in the graph the interference of the shades from nearby trees, as the values decrease before the estimated and the standard insolation.

At last, the velocity data presented in Fig. 5 shows the effect of natural convection: the air gets heated on the solar collector during the day, causing a density difference that, in turn, provokes an upward movement making the air exit the dryer from the chimney. Knowing the outflow air velocity, it is possible to calculate the inflow velocity by knowing the dryer's geometry and the mass flow rate by knowing the density of the fluid.

3.1 Temperature and efficiency results

Fig. 6 compares the temperature results with the measured values. The hourly error is also presented. Note that for the error analysis, only the values between 07:00 and 17:00 was considered since this is the period in which there is insolation.

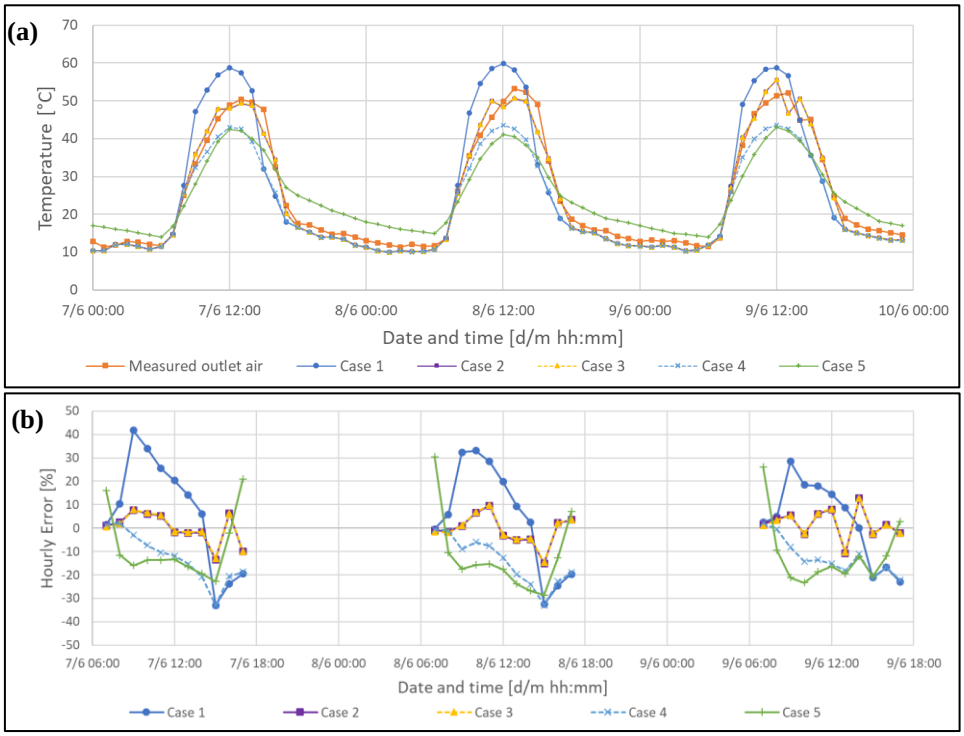

Figure 6. (a) Outlet air temperature estimations, and (b) hourly moving error.

The daily average percentage error and the total average error are presented in Tab. 3. The same timeframe of Fig. 6b was considered.

Table 3. Daily and total average percentage error on final temperature prediction.

	07/06/23 error [%]	08/06/23 error [%]	09/06/23 error [%]	Total average error [%]
Case 1	7.04	4.93	3.16	5.0
Case 2	0.02	0.70	1.94	0.4
Case 3	0.08	0.60	1.97	0.5
Case 4	-12.50	-14.10	-12.60	-13.1
Case 5	-8.39	-11.9	-11.3	-10.5

After all the desired temperatures were calculated, Fig. 6a, the percentual error was analyzed to evaluate the results in each case studied. When calculating the average percentage error for each case during the day, an error of 5.0% was obtained on Case 1, 0.4% on Case 2, 0.5% on Case 3, -13.1% on Case 4, and -10.5% on Case 5.

To expand this analysis, Fig. 6b shows the hourly percentage error, and Fig. 6c the average daily error. Firstly, it is possible to see the adversities of the climate when analyzing Fig. 6b and Tab. 3. Each day obtained a different average error, due to wind, clouds, and temperature variations between each day. Moreover, it is possible to see that Case 1 overestimated the temperature during the day. Besides, this is the only case that uses the measured insolation, which was already higher than expected. Therefore, this means that the insolation meter could be defected or poorly used. Besides, since after 15:00, shades affected the measurement, Case 1 underestimated the temperature.

When analyzing Cases 2 and 3, both used standard insolation and estimated the outlet temperatures with the lowest error. Besides, since the error differences between them are slim, the inlet temperature estimation proved to have a satisfactory equivalence. This was expected since the inlet temperature estimation was based on an hourly ratio between the measured ambient temperature and the measured inlet temperature. This ratio can be applied to other situations in which the dryer is located above an asphalt road since this study was performed with the dryer on PUC's parking lot. Past analysis of the dryer, when it was located above the grass, showed that the difference between the inlet temperature and the ambient temperature was lower. Therefore, when comparing Cases 2 and 3, it is expected that the inlet temperature estimations for Cases 4 and 5 were not the key factor that increased the error.

Finally, when analyzing Cases 4 and 5, the insolation estimation was the main source of error. The insolation estimation was below the standard values, resulting in an underestimation of the outlet temperature. Besides, the outlet temperature was considerably similar to the inlet temperature.

Fig. 7 presents the dryer efficiency throughout the 3 days analyzed.

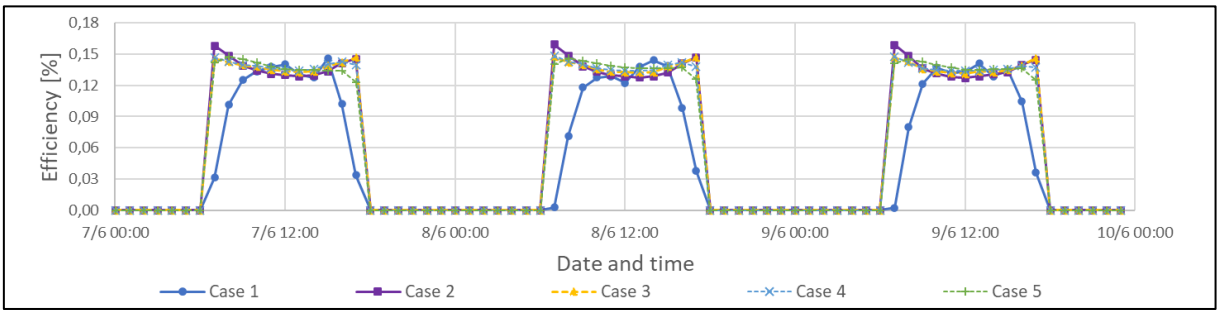

Figure 7. Dryer efficiency results.

The dryer's efficiency results were considerably low, probably due to the date of the experiment, during winter seasons. Although this period is unfavorable for solar drying due to lower insolation and colder wind, it is the best period for simulations and modeling, due to a more stable climate. During the summer, the weather adversities are more intense, resulting in a more unpredictable environment (Cruz and Maia, 2022).

3.2 Geometry optimizing influence

Independently of the case chosen to be used, it is possible to analyze the dryer geometry to guide the project design before building it. As an example, Cases 2 and 5 were chosen to analyze the final temperature and the efficiency results when changing the plate-cover spacing, Fig. 8a, and the solar collector width, Fig. 8b. Both of these geometry parameters were chosen as an example to illustrate the capability of the algorithm for future geometry optimization. Besides, these two Cases were chosen due to their difference in the final percentage error and to assess their relevance for decision-making on geometry optimization.

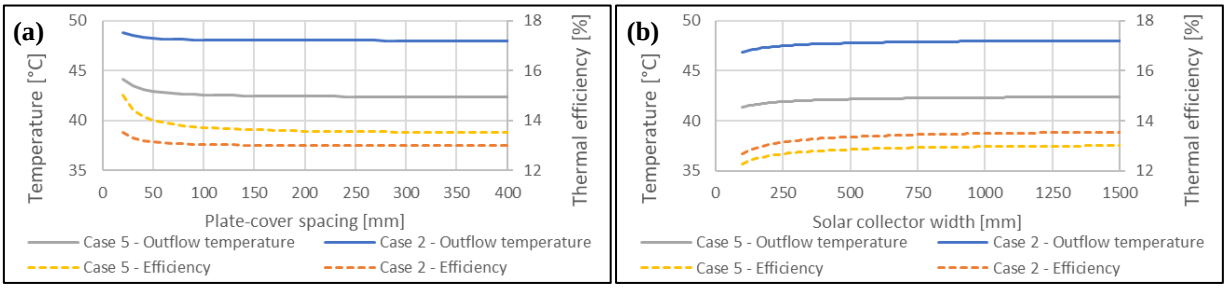

Figure 8. (a) Plate-cover spacing analysis and (b) solar collector width analysis.

Firstly, as already seen in the temperature analysis, when using different Cases, different results are obtained. But when analyzing Fig. 8, it is evident that the overall results can be used as a tool to design the dryer. Traditionally, solar dryers presented by Duffie and Beckman (2013) have a narrow plate-cover spacing, measuring less than 100 mm. This is understandable, as seen in Fig. 8a, since the efficiency and outflow temperature are higher. However, the HSED built at GREEN has a large opening of 350 mm. This hinders the dryer's performance, but this large spacing can be exploited by adding a low reflective plate in the middle.

On the other hand, when analyzing Fig. 8b, it seems that the solar collector width chosen (1.30 m) was successful because, after this value, the dryer's performance did not increase significantly. Therefore, building a wider solar collector would only result in a higher building cost with a negligible performance increase. One plausible explanation is that a large solar collector width increased the heat transfer coefficient loss, despite the increase of useful area for solar energy collecting.

4. CONCLUSIONS

Due to the variety of hybrid solar dryers studied recently, a mathematical algorithm and a drying model of an air heater were developed to analyze the heating performance. A Hybrid Solar-Electric Dryer located at PUC Minas, Belo Horizonte, MG, Brazil, was used to validate the method studied in this work. The final airflow temperature and the dryer's thermal efficiency were calculated with the algorithm developed on an Engineering Equation Solver software. To analyze the computed data, the outflow air temperature was measured during a 3-day period in June of 2023 to be used as the accepted value.

To assess the impact of the ambient temperature and insolation input data on the final results, five case studies were considered, each using progressively less measured environmental data. The results obtained in Case 1 were affected probably due to sensor malfunction and poor handling. The insolation values were above expected for the studied dates, and the sensor location was partially shaded during the evening. However, when using standard insolation (Cases 2 and 3), the error obtained was lower than the uncertainty, meaning that the sensors used can be upgraded for a more precise validation. Besides, this proved that the inlet temperature estimation method was satisfactory. Finally, Cases 4 and 5 underestimated the temperature, obtaining the highest absolute errors. This happened probably due to an underestimation of the insolation. However, this can be calibrated in the algorithm for future analysis.

Independently of the case used, the algorithm proved to be useful for project design. A geometry analysis was performed to evaluate the final temperature and efficiency when changing the solar collector width and the plate-cover spacing. Besides this method can also be applied to compare different materials used in the dryer. For example, if the paint used in the collector has a lower reflectance, it is possible to evaluate the increase in performance and analyze if it is worth the investment. Therefore, the methodology proposed can be used to model air heaters with moderate ease and flexibility.

5. ACKNOWLEDGEMENTS

This study was partially funded by the Coordenação de Aperfeiçoamento de Pessoal de Nível Superior (CAPES), Brazil, finance code 001. The authors are also thankful to PUC Minas, FAPEMIG, and CNPq.

6. REFERENCES

Akpinar, E., 2010. Drying of mint leaves in a solar dryer and under open sun: modelling, performance analyses. Energy Conversion and Management, Vol. 51, No. 12, pp. 2407-2418.

Alfiya, P.V., Murali, S., Aniesrani Delfiya, D.S., Sreelakshmi, K.R., Sivaraman, G.K., Ninan, G., 2022. Kinetics, modelling and evaluation of Bombay duck (Harpodon nehereus) dried in solar-LPG hybrid dryer. Solar Energy, Vol. 242, pp. 70-78.

Barbosa, E.M.C., Maia, C.B., Zidan, D.C., Barbosa, R.R.C., Santana V.A.C. and Diniz A.S.A.C., 2018. "Experimental Analysis of Banana Drying in an Electric Hybrid Solar Dryer". In *Proceedings of the 17th Brazilian Congress of Thermal Engineering and Sciences – ENCIT 2018*. Águas de Lindóia, Brazil.

Bhavsar, H., Patel, C.M., 2023 Performance analysis of cabinet type solar dryer for ginger drying with & without thermal energy storage material. Materials Today: Proceedings, Vol. 73, pp. 595-603.

Chauhan, P.S., Kumar, A., Nuntadusit, C., 2018. Thermo-environomical and drying kinetics of bitter gourd flakes drying under north wall insulated greenhouse dryer. Solar Energy, Vol. 162, pp. 205-216.

Crawley, D.B., Huang, Y.J., 1997. Does it matter which weather data you use in energy simulations? Building Energy Simulation User News, Vol. 18, No. 1.

Cruz, G.M.B, Maia, C.B., 2022. "Thermodynamic Modeling of a Hybrid Solar-Electric Dryer". In *Proceedings of the 19th Brazilian Congress of Thermal Engineering and Sciences – ENCIT 2022*. Bento Gonçalves, Brazil.

Dake, R.A., N'Tsoukpoe. K.E., Kuznik, F., Lèye, B., Ouédraogo, I.W.K., 2021 A review on the use of sorption materials in solar dryers. Renewable Energy, Vol. 175, pp. 965-979.

Dhanushkodi, S., Wilson, V. H., Sudhakar, K., 2017. Mathematical modeling of drying behavior of cashew in a solar biomass hybrid dryer. Resource-Efficient Technologies, Vol. 3, No. 4, pp. 359-364.

Duffie J.A. and Beckman W.A., 2013. *Solar Engineering of Thermal Processes*. John Wiley & Sons, Inc., Hoboken, Unites States of America, 4th edition.

Erbs, D.G., Klein, S.A., Duffie, J.A., 1982. Estimation of the Diffuse Radiation Fraction for Hourly, Daily, and Monthly-Average Global Radiation. Solar Energy, Vol. 28, No. 4, pp. 293-302.

Hadibi, T. et al., 2021. 3E analysis and mathematical modelling of garlic drying process in a hybrid solar-electric dryer. Renewable Energy, Vol. 170, pp. 1052-1069.

Malakar, S., Alam, M., Arora, V.K., 2022. Evacuated tube solar and sun drying of beetroot slices: Comparative assessment of thermal performance, drying kinetics, and quality analysis. Solar Energy, Vol. 233, pp. 246-258.

Martins, F.R., Pereira, E.B., Abreu, S.L., 2007. Satellite-derived solar resource maps for Brazil under SWERA. Project. Solar Energy, Vol. 81, pp. 517-528.

Mühlbauer, W., Müller, J., 2020. *Drying Atlas: Drying Kinetics and Quality of Agricultural Products*. Woodhead Publishing, an imprint of Elsevier, Duxford, 1st edition.

Murali, S., Alfiya, P.V., Aniesrani Delfiya, D.S., Harikrishnan, S., Kunjulakshmi, S., Samuel, M.P., 2022. Performance evaluation of PV powered solar tunnel dryer integrated with a mobile alert system for shrimp drying. Solar Energy, Vol. 240, pp. 246-257.

Roratto, T.B., Monteiro R.L., Carciofi, B.A.M. and Laurindo, J.B., 2021. An innovative hybrid-solar-vacuum dryer to produce high-quality dried fruits and vegetables. LWT, Vol. 140, No. 110777.

Tiwari, S., Tiwari, G.N, 2016. Thermal analysis of photovoltaic-thermal (PVT) single slope roof integrated greenhouse solar dryer. Solar Energy, Vol. 138, pp. 128-136.

7. RESPONSIBILITY NOTICE

The authors are the only responsible for the printed material included in this paper.